JOURNAL OF SOLID STATE CHEMISTRY **140,** 14–19 (1998)
ARTICLE NO. SC987798

Synthesis and Magnetic Properties of New Series of One-Dimensional Oxides $Ca_3Co_{1+x}B_{1-x}O_6$ (B = Ir, Ru)

Hiroshi Kageyama,[1] Kazuyoshi Yoshimura, and Koji Kosuge

Department of Chemistry, Graduate School of Science, Kyoto University, Kyoto 606-8502, Japan

Received June 30, 1997; in revised form February 19, 1998; accepted February 24, 1998

New one-dimensional compounds Ca_3CoBO_6 (B = Ir, Ru) with K_4CdCl_6-type structure have been synthesized by conventional solid state reactions. Both compounds adopt the rhombohedral symmetry with the space group $R\bar{3}c$; a = 9.1811(1) Å, c = 10.8232(3) Å, Z = 6 (hexagonal expression) for Ca_3CoIrO_6 and a = 9.1921(3) Å, c = 10.7784(7) Å, Z = 6 for Ca_3CoRuO_6. One-dimensional chains are built by alternating face-shared CoO_6 octahedra and BO_6 trigonal prisms. The magnetic susceptibility of Ca_3CoIrO_6 shows an abrupt drop at 30 K, as seen in the case of Sr_3NiIrO_6, suggesting that ferromagnetic chains couple antiferromagnetically. On the contrary, Ca_3CoRuO_6 is an ordinary antiferromagnet with T_N = 55 K. We have also succeeded in preparing the solid solution series, $Ca_3Co_{1+x}Ir_{1-x}O_6$ and $Ca_3Co_{1+x}Ru_{1-x}O_6$ ($0 \le x \le 1$), and magnetic properties of these systems were investigated. © 1998 Academic Press

1. INTRODUCTION

Since the discovery of Sr_3CuPtO_6 (1), the structure of which is related to the one of K_4CdCl_6 (2), many compounds with the general formula A'_3ABO_6 (A' = Sr, Ca, … ; A = Ni, Cu, Zn, … ; B = Ir, Pt, Ru, …) have been synthesized and investigated from the viewpoints of their structures and magnetic properties (3–12). Figure 1a shows the perspective view of A'_3ABO_6-type structure along the hexagonal [110] direction, which consists of infinite chains of alternating face-sharing AO_6 trigonal prisms (A site) and BO_6 octahedra (anti-trigonal prisms, B site). A one-dimensional (1-D) magnetic character is expected because the AO_3–BO_3 chains are separated by the A' ions. The members of the A'_3ABO_6 family are known to show various magnetic behaviors, some of which are discussed in terms of the 1-D magnetic models, such as a random quantum spin chain paramagnet model for $Sr_3CuPt_{0.5}Ir_{0.5}O_6$ (6), a 1-D Heisenberg model for Sr_3CuPtO_6 (4), and a 1-D Ising model for Sr_3ZnIrO_6 (8). Another structural feature of this family is that each AO_3–BO_3 chain is surrounded by six chains, thus forming a triangular net as seen in Fig. 1b. Therefore we also expect cooperative phenomena caused by the triangular arrangement of the chains.

Recently, the crystal structure of $Ca_3Co_2O_6$ was determined by Fjellvåg *et al.* (9); $Ca_3Co_2O_6$ is isostructural with Sr_3ZnIrO_6 (8), and the Co ions occupy both the A and the B sites. The ferromagnetic Ising-spin chains order ferrimagnetically on the triangular lattice below 25 K as a result of the antiferromagnetic interaction between the chains (11–13). Furthermore, by our Mössbauer measurements of $Ca_3(Co_{0.99}{}^{57}Fe_{0.01})_2O_6$, the quantum levels of Fe^{3+} ions were first observed in magnetically dense systems (14). This remarkable observation is attributed to the large difference between magnetic characters of the host (Ising) and impurity (Heisenberg) spins.

Encouraged by the peculiar magnetic properties on $Ca_3Co_2O_6$, we tried to synthesize Co-contained compounds of this structure series. As a result, new compounds with the chemical formula Ca_3CoIrO_6 and Ca_3CoRuO_6 were successfully prepared. As expected, the solid solution series of $Ca_3Co_{1+x}Ir_{1-x}O_6$ and $Ca_3Co_{1+x}Ru_{1-x}O_6$ ($0 \le x \le 1$) were also prepared. Here we report the synthesis, structures, and magnetic properties of these systems.

2. EXPERIMENTAL

Polycrystalline compounds of $Ca_3Co_{1+x}Ir_{1-x}O_6$ and $Ca_3Co_{1+x}Ru_{1-x}O_6$ ($0 \le x \le 1$) were prepared by conventional solid state reactions. The stoichiometric amounts of reagents $CaCO_3$ (99.99%), CoO (99.99%), Ir (99.9%), and Ru (99.99%) were sufficiently mixed using an agate mortar, pressed into pellets and calcined in air at 1173 K for one day. Then, the samples were heated in air for 1 or 2 weeks at temperatures in the range 1273–1423 K for $Ca_3Co_{1+x}Ir_{1-x}O_6$ and 1273–1500 K for $Ca_3Co_{1+x}Ru_{1-x}O_6$ with intermediate grindings. Because $Ca_3Co_2O_6$ decomposes to CaO and CoO at 1299 K (15), lower temperatures are required for the preparation of the samples with small x.

[1] Present address: Institute for Solid State Physics, University of Tokyo, Roppongi, Minato-ku, Tokyo 106-8666, Japan. E-mail: kage@issp.u-tokyo.ac.jp.

0022-4596/98 $25.00

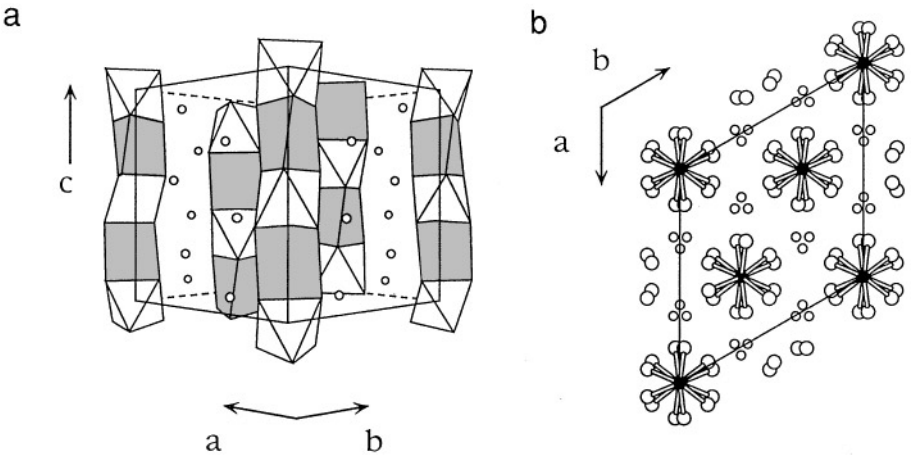

FIG. 1. Schematic illustration of the structure of A'_3ABO_6. (a) The perspective view along the [110] direction. The open and shaded polyhedra represent BO_6 octahedra (anti-trigonal prisms) and AO_6 trigonal prisms, respectively. The open circles show A' atoms. (b) The projection along the c axis. The black circles represent A' and B atoms, the large open circles represents the oxygen, and the small open circles represent A atoms.

Powder samples were structurally characterized using a high power (18 kW) X-ray diffractometer (Mac Science, M18XHF22) with Cu$K\alpha$ radiation, $\lambda = 1.5405$ Å. Data were recorded in steps of 0.02° in 2θ between 5° and 80° (Bragg Brentano geometry) and the counting time was 0.1 sec. The unit-cell parameters were determined by the least-square fitting to some characteristic indexes in the powder X-ray diffraction patterns. The Rietveld analysis (16) of the powder X-ray diffraction data of the end compounds Ca_3CoIrO_6 and Ca_3CoRuO_6 was performed using the refinement package Rietan (17). The structure of Sr_3NiIrO_6 was used as a starting model. Data for the Rietveld refinements were collected over $5^\circ \leq 2\theta \leq 80^\circ$ in 0.02° steps, with integration times of 1.0 sec.

From the thermogravimetric analysis measured between 300 and 1273 K in flowing O_2, the weight change was found to be within 0.1 wt% for all the samples. Considering that fact, it can be assumed that the oxygen content is almost stoichiometric (i.e., 5.97–6.00).

Magnetic properties were measured on powder samples using a Quantum Design MPMS SQUID magnetometer. Measurements were carried out in various magnetic fields in the temperature range of $4\text{ K} \leq T \leq 300\text{ K}$ after cooling the sample in zero magnetic field (zero-field cooled, ZFC) and also after cooling in the measuring field (field cooled, FC). Magnetic susceptibility in the high-temperature range $300\text{ K} \leq T \leq 770\text{ K}$ was measured at $H = 0.5$ T using a torsion magnetic balance.

3. RESULT AND DISCUSSION

Crystal Structure

The powder XRD pattern of Ca_3CoIrO_6 is shown in Fig. 2. Although an unknown impurity phase was observed (see the peak around at 37.5°), its XRD intensity is very small so that it would not disturb any intrinsic magnetic properties of Ca_3CoIrO_6. The powder X-ray Rietveld refinement was carried out for Ca_3CoIrO_6 both in the space group of Sr_3ZnIrO_6 (8), $R\bar{3}c$, and in that of the structurally related Sr_3CuPtO_6 (3), $C2/c$. All attempts to refine in the monoclinic space group diverged. On the other hand, refinement of the rhombohedral space group $R\bar{3}c$ gave a unit cell of $a = 9.1811(1)$ Å and $c = 10.8232(3)$ Å and quickly converged to $R_{wp} = 14.5\%$ and $R_p = 12.3\%$. Here we assumed that the Co and the Ir ions occupy the A and the B sites, respectively, that is, the chain consists of alternating face-sharing CoO_6 trigonal prisms and IrO_6 octahedra. Observed and calculated interplanar spacings and intensities of Ca_3CoIrO_6 are given in Table 1. It is likely that the poor convergency is the result of the preferred orientation of the sample as is often seen in the case of one-dimensional

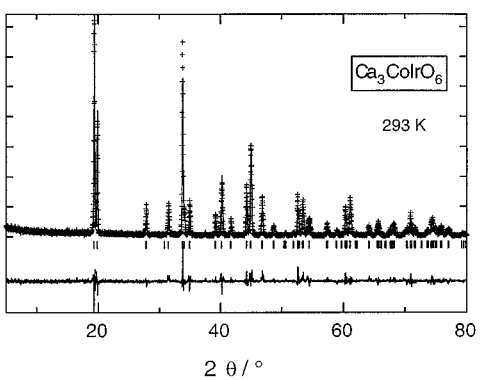

FIG. 2. X-ray Rietveld analysis for Ca_3CIrO_6 showing the observed, calculated, and difference patterns.

TABLE 1
Observed and Calculated Powder XRD of Ca_3CoIrO_6
($R\bar{3}c$, $a = 9.1811$ Å, $c = 10.8232$ Å)

hkl	d_{obs}	d_{cacl}	I/I_0(obs)	I/I_0(calc)
110	4.5904	4.5906	100	100
012	4.4755	4.4737	50	50
202	3.2087	3.2039	15	26
113	2.8412	2.8366	14	13
300	2.6527	2.6504	99	88
122	2.6300	2.6273	13	21
104	2.5644	2.5615	14	15
220	2.2985	2.2953	11	8
024	2.2403	2.2369	25	28
131	2.1641	2.1608	8	5
312	2.0448	2.0422	27	20
214	2.0145	2.0108	46	43
223	1.9395	1.9366	20	13
042	1.8696	1.8659	4	5
321	1.8031	1.7987	2	1
125	1.7615	1.7564	1	1
410	1.7379}	1.7351	23}	14
232		1.7285		2
134	1.7125	1.7094	17	18
116	1.6828	1.6789	7	11
404	1.6050	1.6020	6	7
413	1.5667}	1.5636	3}	1
143		1.5636		1

compounds (4). In addition, a small amount of Ir may be lost as IrO_3 because of high volatility. Although several attempts were made to refine the fitting by varying site occupancies e.g., the deficiencies and/or the substitution in the Ir site, these did not improve the result.

The representative powder XRD patterns for $Ca_3Co_{1+x}Ir_{1-x}O_6$ are shown in Fig. 3. It is clear that the synthesis of $Ca_3Co_{1+x}Ir_{1-x}O_6$ solid solution series is successful for the whole range of x ($0 \le x \le 1$). The top of Fig. 4 represents the crystallographic unit-cell parameters with the hexagonal expression as a function of composition x. The lattice parameters [$a = 9.0710(1)$ Å, $c = 10.3751(2)$ Å] for $Ca_3Co_2O_6$ are almost in good agreement with those previously reported (9). Both a and c shrink with increasing x. The Ir and the Co ions are considered to be distributed randomly on the B site because the XRD pattern has no additional peak which indicates the existence of ordering between the Ir and the Co ions at the B site.

Next, the representative powder XRD patterns for $Ca_3Co_{1+x}Ru_{1-x}O_6$ are shown in Fig. 5, which tells us the successful synthesis of the Ru-based solid solution. No impurity was detected for $x \ge 0.1$ from the XRD patterns, whereas, as for $x = 0$ (Ca_3CoRuO_6), a small amount of $CaRuO_3$ was detected as marked by asterisks in Fig. 5. The powder X-ray Rietveld refinement for Ca_3CoRuO_6 was performed in the space groups of $R\bar{3}c$ and $C2/c$, where the

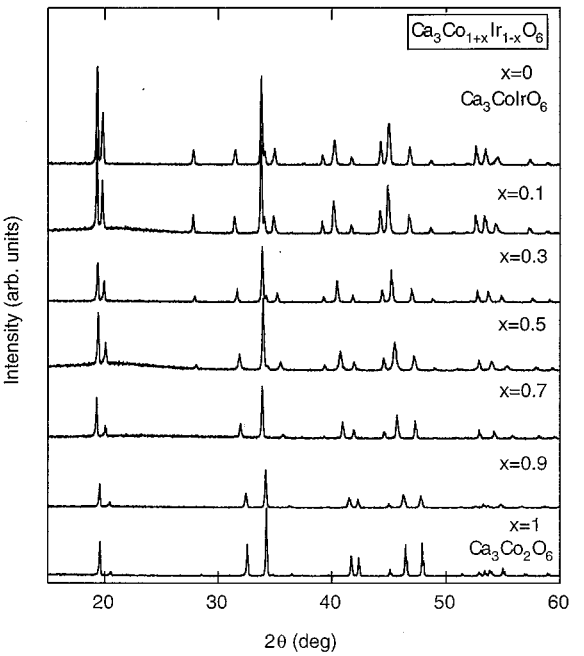

FIG. 3. Observed powder XRD pattens for $Ca_3Co_{1+x}Ir_{1-x}O_6$.

Co and the Ru ions are assumed to occupy the A and the B sites, respectively. The result is the same as that for Ca_3CoIrO_6; only the refinement in the former space group of $R\bar{3}c$ converged to $R_{wp} = 15.5\%$ and $R_p = 17.5\%$, giving

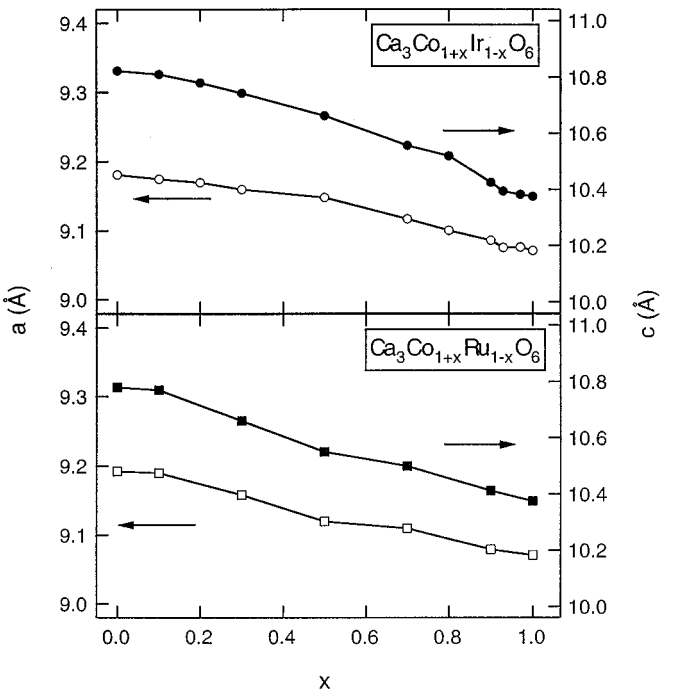

FIG. 4. Crystallographic unit-cell parameters as a function of composition x in the $Ca_3Co_{1+x}Ir_{1-x}O_6$ (top) and $Ca_3Co_{1+x}Ru_{1-x}O_6$ (bottom) solid solution series. The errors on cell constants for the samples with $0 < x < 1$ are within 0.001 Å.

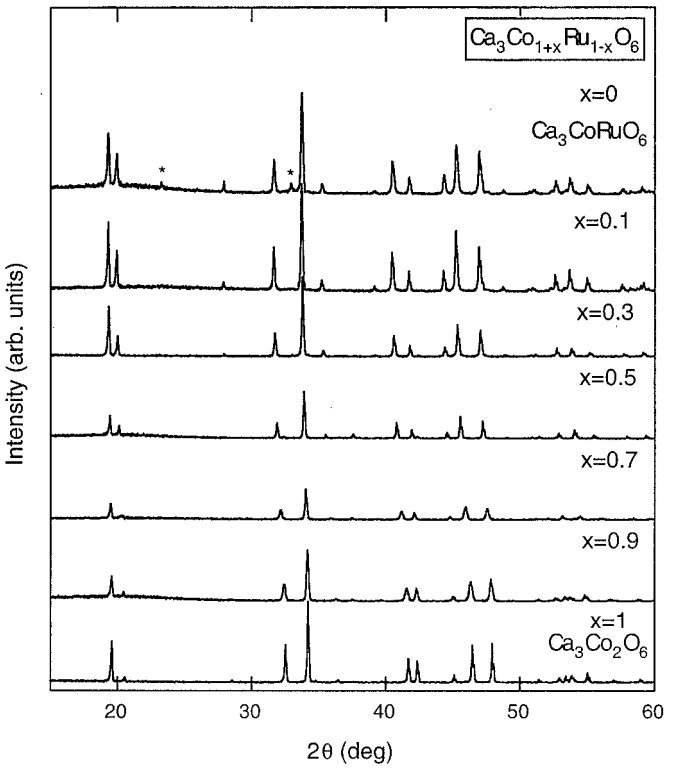

FIG. 5. Observed XRD patterns for $Ca_3Co_{1+x}Ru_{1-x}O_6$. The peaks marked by asterisk correspond to $CaRuO_3$.

TABLE 2
Observed and Calculated Powder XRD of Ca_3CoRuO_6 ($R\bar{3}c$, $a = 9.1921$ Å, $c = 10.7784$ Å)

hkl	d_{obs}	d_{calc}	I/I_0(obs)	I/I_0(calc)
110	4.5997	4.5960	56	72
012	4.4535	4.4513	29	30
*	3.8241	—	4	—
202	3.1974	3.1975	5	4
113	2.8255	2.8240	40	28
*	2.7168	—	7	—
300	2.6543	2.6535	100	100
122	2.6271	2.6248	2	2
104	2.5447	2.5438	9	11
220	2.2990	2.2980	4	4
024	2.2266	2.2257	37	33
131	2.1632	2.1626	18	11
312	2.0430	2.0420	20	14
214	2.0044	2.0032	60	55
223	1.9349	1.9338	46	34
042	1.8668	1.8661	4	1
321	1.8011	1.8004	2	2
006	1.7906	1.7897	3	2
125	1.7379}	1.7480	17}	2
410		1.7371		14
134	1.7060	1.7052	21	18
116	1.6687	1.6678	7	9
404	1.5994	1.5988	6	6
413	1.5667}	1.5628	3}	5
143		1.5628		2

The asterisks correspond to the peaks of $CaRuO_3$.

lattice parameters of $a = 9.1921(3)$ Å and $c = 10.7784(7)$ Å. Observed and calculated interplanar spacings and intensities of Ca_3CoRuO_6 are given in Table 2. The reason for the poor convergency is also attributable to the sample orientation and the volatility of RuO_4 at high temperatures. The composition dependence of the unit-cell parameters for the Ca_3CoRuO_6 solid solution series is shown at the bottom of Fig. 4. As in $Ca_3Co_{1+x}Ir_{1-x}O_6$, both a and c decrease with increasing x.

Magnetic Properties

In contrast to the similar composition dependence of the unit-cell parameters between the Ir- and Ru-based solid solutions, magnetically, the two systems differ significantly. The temperature dependence of magnetic susceptibility M/H for Ca_3CoIrO_6 measured at 0.5, 1.0, and 5.0 T is shown in Fig. 6. The M/H vs. T curves obey the Curie–Weiss law above 200 K. The positive value of the Weiss temperature ($T_W = 165$ K) implies the ferromagnetic intrachain interaction. The observed paramagnetic Bohr-magneton number $P_{eff} = 3.73\,\mu_B$/f.u. is close to the theoretical value of $4.24\,\mu_B$ for $S = 3/2$ (Co^{2+}, high spin) and $S = 1/2$ (Ir^{4+}). However, it should be noted that the analysis using the data of powder samples involves ambiguity because electron spin characters in low-dimensional magnets are often highly anisotropic, and thus an observed magnetization gives an averaged one over the three crystallographic axes. Add to this that there may be an orbital contribution to the effective spin moment. Therefore, the measurements using a single crystal or an aligned sample are necessary in order to make quantitative analysis.

Below 150 K, there is a positive deviation from the Curie–Weiss law. The value of M/H depends on H for $T \leq 80$ K. For the ZFC sample, there is a precipitous drop in the magnetization at $T_c = 32$ K to that of a constant low value for $T < 25$ K. Below T_c, the irreversibility in M/H vs. T curves appears between ZFC and FC processes, indicating that a ground state is not a spin singlet state but (canted) antiferromagnetic state. It can be deducible that ferromagnetic chains couple antiferromagnetically below T_c, which can explain the sharp drop in the magnetization. According to Ref. 5, Sr_3NiIrO_6 shows a similar magnetic behavior to Ca_3CoIrO_6: the M/H vs. T obeys the Curie–Weiss law at high temperatures, for $70\text{ K} < T < 150$ K there is a positive deviation from the Curie–Weiss law, and at temperatures below $T_c = 21$ K there is a precipitous drop in the magnetization. Nguyen *et al.* suggested from the abrupt drop in the magnetization at T_c that this material should achieve a singlet ground state (5). However, they performed only ZFC

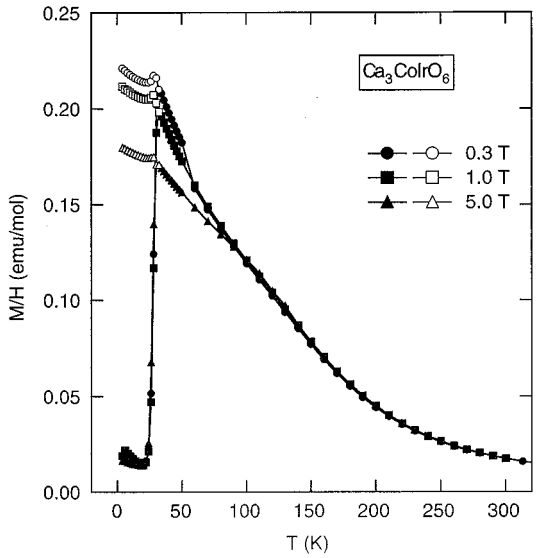

FIG. 6. M/H vs. T curves of Ca_3CoIrO_6 measured in a field of 0.3, 1.0, and 5.0 T. Solid marks represent ZFC, and open marks represent FC.

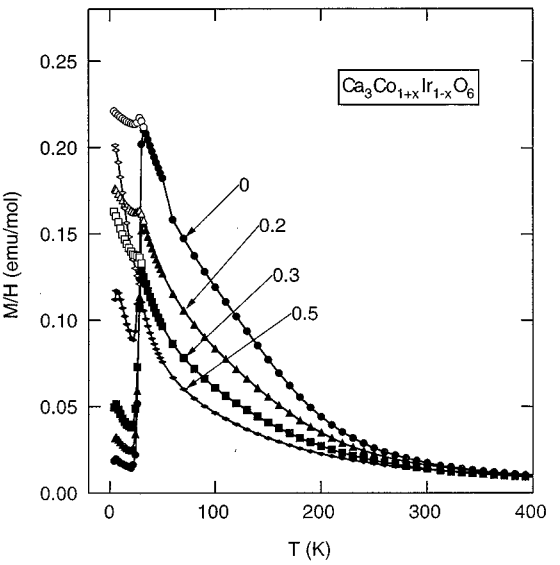

FIG. 7. Temperature dependence of magnetic susceptibilities M/H at $H = 0.5$ T for $Ca_3Co_{1+x}Ir_{1-x}O_6$ ($x \leq 0.5$). Solid marks represent ZFC, and open marks represent FC.

magnetization measurements. We performed the FC and ZFC magnetization measurements on Sr_3NiIrO_6 and found that Sr_3NiIrO_6 also exhibits FC and ZFC divergency at T_c. Consequently, both Ca_3CoIrO_6 and Sr_3NiIrO_6 are considered as canted antiferromagnets below T_c, even though the neutron diffraction study for Sr_3NiIrO_6 failed to observe magnetic Bragg peaks at low temperatures (5). There are many Ir-based compounds in this family such as Sr_3CaIrO_6, Sr_3CuIrO_6, and Sr_3CdIrO_6 (5, 7, 8), but only Ca_3CoIrO_6 and Sr_3NiIrO_6 show such complex magnetic behaviors. We do not presently give an explanation for the difference in the magnetic behaviors of two compounds and the others. Further study is needed in order to make clear the magnetic structure of Ca_3CoIrO_6 and Sr_3NiIrO_6.

The temperature dependence of magnetic susceptibility for $Ca_3Co_{1+x}Ir_{1-x}O_6$ are shown in Figs. 7 and 8, for $x \leq 0.5$ and $x > 0.5$, respectively. The magnetic susceptibility in the high-temperature range can be fitted to the Curie–Weiss law for all x. In Fig. 9, the composition dependence of T_W and P_{eff} is presented. As x increases, the value of T_W decreases for $x < 0.7$ and then increases. P_{eff} increases monotonously with x. The abrupt drop in the M/H curves appears for the ZFC samples with $x \leq 0.5$. Remarkable future is that T_c is almost independent of x; for $Ca_3Co_{1.5}Ir_{0.5}O_6$, T_c is 28 K only 4 K lower than in the case of the end compound Ca_3CoIrO_6. Although in the case of Ca_3CoIrO_6 the deviation from the Curie–Weiss law for $70\,K < T < 200\,K$ was obtained as mentioned previously, such anomaly was not observed for $x = 0.2$, 0.3, and 0.5. For $x > 0.5$, an abrupt drop in the magnetization disappears. Instead, there is a broad maximum in the M/H vs. T curves around 10 K. The decrease of T_W with x would be accounted for the disappearance of T_c. When the ferromagnetic intrachain interaction becomes smaller, the interchain interaction would also get weak. This would prevent the ferromagnetic chains from coupling antiferromagnetically. As shown in the inset of Fig. 8, the abrupt increase in magnetization was observed for $x \geq 0.97$, which corresponds to the transition from a paramagnetic state to a ferrimagnetic state (11–13).

In Fig. 10, we show the temperature dependence of the magnetic susceptibility of $Ca_3Co_{1+x}Ru_{1-x}O_6$ solid

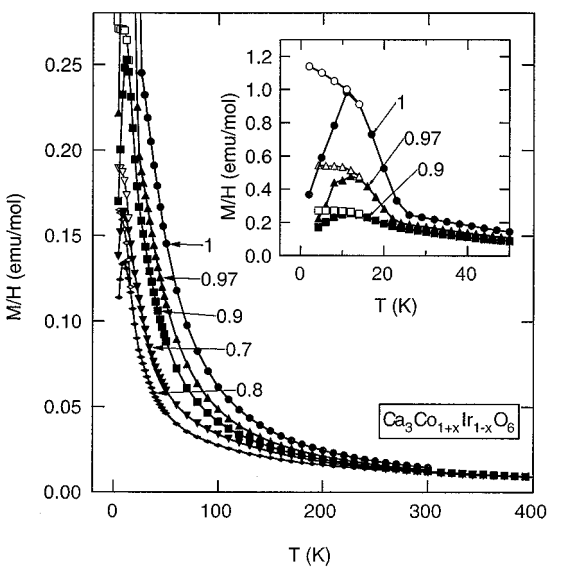

FIG. 8. Temperature dependence of magnetic susceptibilities M/H at $H = 0.5$ T for $Ca_3Co_{1+x}Ir_{1-x}O_6$ ($x > 0.5$). Solid marks represent ZFC, and open marks represent FC. Inset: Enlarged plot for $x = 0.9$, 0.97, and 1.

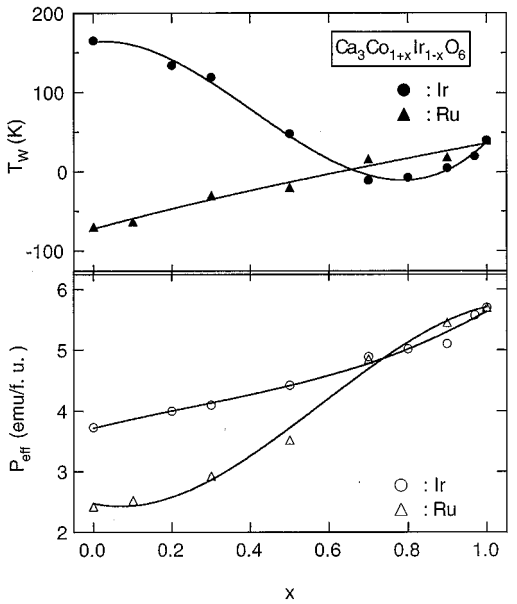

FIG. 9. Weiss temperature T_W and P_{eff} per formula unit of $Ca_3Co_{1+x}B_{1-x}O_6$ (B = Ir, Ru) as a function of composition x. Solid curves are guides to the eye.

solution series. Above 100 K, the M/H vs. T curves were well fitted to the Curie–Weiss law. The composition variations of T_W and P_{eff} are shown in Fig. 8. Both T_W and P_{eff} increase consistently with x. $P_{eff} = 2.42\,\mu_B$/f.u for Ca_3CoRuO_6 supports the spin configuration of $S = 1/2$ (Co^{2+}, low spin) and S = 1 (Ru^{4+}) which gives $3.00\,\mu_B$. Note that this model holds if spin characters are isotropic as mentioned previously.

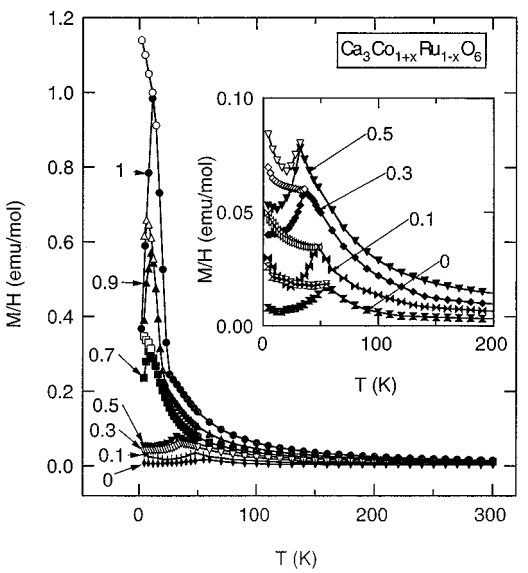

FIG. 10. Temperature dependence of magnetic susceptibilities M/H at $H = 0.5$ T for $Ca_3Co_{1+x}Ru_{1-x}O_6$. Solid marks represent ZFC, and open marks represent FC. For ($x \leq 0.5$), only ZFC process are presented. Inset: Enlarged plot for $0 \leq x \leq 0.5$.

Magnetic susceptibility for $x = 0$, 0.1, 0.3, and 0.5 displays an ordinary antiferromagnetic transition. The antiferromagnetic ordering temperature T_N decreases with x; $T_N = 55$, 50, 36, and 34 K for $x = 0$, 0.1, 0.3 and 0.5, respectively, which is consistent with the composition variation of T_W (Fig. 9). For the samples with $x > 0.7$, there is a broad maximum in the M/H vs. T curves around 10 K. This broad maximum is also observed in the case of $Ca_3Co_{1+x}Ir_{1-x}O_6$.

4. SUMMARY

We have prepared the new series of one-dimensional oxides $Ca_3Co_{1+x}B_{1-x}O_6$ (B = Ir, Ru) isostructural with Sr_3ZnIrO_6. Ca_3CoIrO_6 shows the abrupt drop in the magnetic susceptibility at 30 K, as in the case of Sr_3NiIrO_6, suggesting that the ferromagnetic chains couple antiferromagnetically. On the contrary, Ca_3CoRuO_6 is an ordinary antiferromagnet with $T_N = 55$ K. For the further understanding of the magnetism on these compounds, the comparison with other Ir- and Ru-based compounds would be important. We have succeeded in preparing a new Ir-based compound Sr_3CoIrO_6, whose structure and magnetic properties will be published elsewhere. Attempts to synthesize other Ru-based compounds such as Ca_3NiIrO_6, Sr_3CoRuO_6, and Sr_3ZnRuO_6 were all unsuccessful.

REFERENCES

1. A. P. Wilkinson, A. K. Cheetham, W. Kunnman, and Å. Kvick, *Eur. J. Solid State Inorg. Chem.* **28**, 453 (1991).
2. G. Bergerhoff and O. Schmitz-Dumott, *Z. Anorg. Allg. Chem.* **284,** 10 (1956).
3. J. L. Hodeau, H. Y. Tu, P. Bordet, T. Fournier, P. Strobel, M. Marezio, and G. V. Chandrashekhar, *Acta Cryst.* **B48,** 1 (1992).
4. T. N. Nguyen, D. M. Giaquinta, and H.-C. zur Loye, *Chem. Mater.* **6,** 1642 (1994).
5. T. N. Nguyen and H. C. zur Loye, *J. Solid State Chem.* **117,** 300 (1995).
6. T. N. Nguyen, P. A. Lee, and H.-C. zur Loye, *Science* **271,** 489 (1996).
7. N. Segal, J. F. Vente, T. S. Bush, and P. D. Battle, *J. Mater. Chem.* **6,** 395 (1996).
8. C. Lampe-Önnerud, M. Sigrist, and H.-C zur Loye, *J. Solid State Chem.* **127,** 25 (1995).
9. H. Fjellvåg, E. Gulbrandsen, S. Aasland, A. Oslen, and B. C. Haucack, *J. Solid State Chem.* **124,** 190 (1996).
10. J. Darriet, F. Grasset, and P. D. Battle, *Mater. Res. Bull.* **32,** 139 (1997).
11. S. Aasland, H. Fjellvåg, and B. Hauback, *Solid State Commun.* **101,** 187 (1997).
12. H. Kageyama, J. Yoshimura, K. Kosuge, H. Mitamura, and T. Goto, *J. Phys. Soc. Jpn.* **66,** 1607 (1997).
13. H. Kageyama, K. Yoshimura, K. Kosuge, M. Azuma, M. Takano, H. Mitamura, and T. Goto, *J. Phys. Soc. Jpn.* **66,** 3996 (1997).
14. H. Kageyama, S. Kawasaki, K. Mibu, M. Takano, K. Yoshimura, and K. Kosuge, *Phys. Rev. Lett.* **79,** 3258 (1997).
15. E. Wocrmann and A. Muan, *J. Inorg. Nucl. Chem.* **32,** 1457 (1970).
16. H. M. Rietveld, *J. Appl. Crystallogr.* **2,** 65 (1969).
17. F. Izumi, "The Rietveld Method" (R. A. Young, Ed.). Oxford University Press, Oxford (1993), Chap. 13; Y.-I. Kim and F. Izumi, *J. Ceram. Soc. Jpn.* **102,** 401 (1994).